PHYSICAL REVIEW C **70**, 044901 (2004)

Centrality and pseudorapidity dependence of charged hadron production at intermediate p_T in Au+Au collisions at $\sqrt{s_{NN}}=130$ GeV

J. Adams,[2] M. M. Aggarwal,[28] Z. Ahammed,[42] J. Amonett,[19] B. D. Anderson,[19] D. Arkhipkin,[12] G. S. Averichev,[11] Y. Bai,[26] J. Balewski,[16] O. Barannikova,[31] L. S. Barnby,[2] J. Baudot,[17] S. Bekele,[27] V. V. Belaga,[11] R. Bellwied,[45] J. Berger,[13] B. I. Bezverkhny,[47] S. Bharadwaj,[32] V. S. Bhatia,[28] H. Bichsel,[44] A. Billmeier,[45] L. C. Bland,[3] C. O. Blyth,[2] B. E. Bonner,[33] M. Botje,[26] A. Boucham,[37] A. Brandin,[24] A. Bravar,[3] M. Bystersky,[10] R. V. Cadman,[1] X. Z. Cai,[36] H. Caines,[47] M. Calderón de la Barca Sánchez,[3] J. Carroll,[20] J. Castillo,[20] D. Cebra,[6] P. Chaloupka,[10] S. Chattopdhyay,[42] H. F. Chen,[35] Y. Chen,[7] J. Cheng,[40] M. Cherney,[9] A. Chikanian,[47] W. Christie,[3] J. P. Coffin,[17] T. M. Cormier,[45] J. G. Cramer,[44] H. J. Crawford,[5] D. Das,[42] S. Das,[42] M. M. de Moura,[34] A. A. Derevschikov,[30] L. Didenko,[3] T. Dietel,[13] W. J. Dong,[7] X. Dong,[35] J. E. Draper,[6] F. Du,[47] A. K. Dubey,[14] V. B. Dunin,[11] J. C. Dunlop,[3] M. R. Dutta Mazumdar,[42] V. Eckardt,[22] W. R. Edwards,[20] L. G. Efimov,[11] V. Emelianov,[24] J. Engelage,[5] G. Eppley,[33] B. Erazmus,[37] M. Estienne,[37] P. Fachini,[3] J. Faivre,[17] R. Fatemi,[16] J. Fedorisin,[11] K. Filimonov,[20] P. Filip,[10] E. Finch,[47] V. Fine,[3] Y. Fisyak,[3] K. J. Foley,[3] K. Fomenko,[11] J. Fu,[40] C. A. Gagliardi,[38] J. Gans,[47] M. S. Ganti,[42] L. Gaudichet,[37] F. Geurts,[33] V. Ghazikhanian,[7] P. Ghosh,[42] J. E. Gonzalez,[7] O. Grachov,[45] O. Grebenyuk,[26] D. Grosnick,[41] S. M. Guertin,[7] A. Gupta,[18] T. D. Gutierrez,[6] T. J. Hallman,[3] A. Hamed,[45] D. Hardtke,[20] J. W. Harris,[47] M. Heinz,[47] T. W. Henry,[38] S. Hepplemann,[29] B. Hippolyte,[47] A. Hirsch,[31] E. Hjort,[20] G. W. Hoffmann,[39] H. Z. Huang,[7] S. L. Huang,[35] E. W. Hughes,[4] T. J. Humanic,[27] G. Igo,[7] A. Ishihara,[39] P. Jacobs,[20] W. W. Jacobs,[16] M. Janik,[43] H. Jiang,[7] P. G. Jones,[2] E. G. Judd,[5] S. Kabana,[47] K. Kang,[40] M. Kaplan,[8] D. Keane,[19] V. Yu. Khodyrev,[30] J. Kiryluk,[21] A. Kisiel,[43] E. M. Kislov,[11] J. Klay,[20] S. R. Klein,[20] A. Klyachko,[16] D. D. Koetke,[41] T. Kollegger,[13] M. Kopytine,[19] L. Kotchenda,[24] M. Kramer,[25] P. Kravtsov,[24] V. I. Kravtsov,[30] K. Krueger,[1] C. Kuhn,[17] A. I. Kulikov,[11] A. Kumar,[28] C. L. Kunz,[8] R. Kh. Kutuev,[12] A. A. Kuznetsov,[11] M. A. C. Lamont,[2] J. M. Landgraf,[3] S. Lange,[13] F. Laue,[3] J. Lauret,[3] A. Lebedev,[3] R. Lednicky,[11] S. Lehocka,[11] M. J. LeVine,[3] C. Li,[35] Q. Li,[45] Y. Li,[40] S. J. Lindenbaum,[25] M. A. Lisa,[27] F. Liu,[46] L. Liu,[46] Q. J. Liu,[44] Z. Liu,[46] T. Ljubicic,[3] W. J. Llope,[33] H. Long,[7] R. S. Longacre,[3] M. Lopez-Noriega,[27] W. A. Love,[3] Y. Lu,[46] T. Ludlam,[3] D. Lynn,[3] G. L. Ma,[36] J. G. Ma,[7] Y. G. Ma,[36] D. Magestro,[27] S. Mahajan,[18] D. P. Mahapatra,[14] R. Majka,[47] L. K. Mangotra,[18] R. Manweiler,[41] S. Margetis,[19] C. Markert,[47] L. Martin,[37] J. N. Marx,[20] H. S. Matis,[20] Yu. A. Matulenko,[30] C. J. McClain,[1] T. S. McShane,[9] F. Meissner,[20] Yu. Melnick,[30] A. Meschanin,[30] M. L. Miller,[21] Z. Milosevich,[8] N. G. Minaev,[30] C. Mironov,[19] A. Mischke,[26] D. Mishra,[14] J. Mitchell,[33] B. Mohanty,[42] L. Molnar,[31] C. F. Moore,[39] M. J. Mora-Corral,[22] D. A. Morozov,[30] V. Morozov,[20] M. G. Munhoz,[34] B. K. Nandi,[42] T. K. Nayak,[42] J. M. Nelson,[2] P. K. Netrakanti,[42] V. A. Nikitin,[12] L. V. Nogach,[30] B. Norman,[19] S. B. Nurushev,[30] G. Odyniec,[20] A. Ogawa,[3] V. Okorokov,[24] M. Oldenburg,[20] D. Olson,[20] S. K. Pal,[42] Y. Panebratsev,[11] S. Y. Panitkin,[3] A. I. Pavlinov,[45] T. Pawlak,[43] T. Peitzmann,[26] V. Perevoztchikov,[3] C. Perkins,[5] W. Peryt,[43] V. A. Petrov,[12] S. C. Phatak,[14] R. Picha,[6] M. Planinic,[48] J. Pluta,[43] N. Porile,[31] J. Porter,[3] A. M. Poskanzer,[20] M. Potekhin,[3] E. Potrebenikova,[11] B. V. K. S. Potukuchi,[18] D. Prindle,[44] C. Pruneau,[45] J. Putschke,[22] G. Rai,[20] G. Rakness,[29] R. Raniwala,[32] S. Raniwala,[32] O. Ravel,[37] R. L. Ray,[39] S. V. Razin,[11] D. Reichhold,[31] J. G. Reid,[44] G. Renault,[37] F. Retiere,[20] A. Ridiger,[24] H. G. Ritter,[20] J. B. Roberts,[33] O. V. Rogachevskiy,[11] J. L. Romero,[6] A. Rose,[45] C. Roy,[37] L. Ruan,[35] R. Sahoo,[14] I. Sakrejda,[20] S. Salur,[47] J. Sandweiss,[47] I. Savin,[12] P. S. Sazhin,[11] J. Schambach,[39] R. P. Scharenberg,[31] N. Schmitz,[22] L. S. Schroeder,[20] K. Schweda,[20] J. Seger,[9] P. Seyboth,[22] E. Shahaliev,[11] M. Shao,[35] W. Shao,[4] M. Sharma,[28] W. Q. Shen,[36] K. E. Shestermanov,[30] S. S. Shimanskiy,[11] F. Simon,[22] R. N. Singaraju,[42] G. Skoro,[11] N. Smirnov,[47] R. Snellings,[26] G. Sood,[41] P. Sorensen,[20] J. Sowinski,[16] J. Speltz,[17] H. M. Spinka,[1] B. Srivastava,[31] A. Stadnik,[11] T. D. S. Stanislaus,[41] R. Stock,[13] A. Stolpovsky,[45] M. Strikhanov,[24] B. Stringfellow,[31] A. A. P. Suaide,[34] E. Sugarbaker,[27] C. Suire,[3] M. Sumbera,[10] B. Surrow,[21] T. J. M. Symons,[20] A. Szanto de Toledo,[34] P. Szarwas,[43] A. Tai,[7] J. Takahashi,[34] A. H. Tang,[26] T. Tarnowsky,[31] D. Thein,[7] J. H. Thomas,[20] S. Timoshenko,[24] M. Tokarev,[11] T. A. Trainor,[44] S. Trentalange,[7] R. E. Tribble,[38] O. Tsai,[7] J. Ulery,[31] T. Ullrich,[3] D. G. Underwood,[1] A. Urkinbaev,[11] G. Van Buren,[3] A. M. Vander Molen,[23] R. Varma,[15] I. M. Vasilevski,[12] A. N. Vasiliev,[30] R. Vernet,[17] S. E. Vigdor,[16] Y. P. Viyogi,[42] S. Vokal,[11] M. Vznuzdaev,[24] B. Waggoner,[9] F. Wang,[31] G. Wang,[19] G. Wang,[4] X. L. Wang,[35] Y. Wang,[39] Y. Wang,[40] Z. M. Wang,[35] H. Ward,[39] J. W. Watson,[19] J. C. Webb,[16] R. Wells,[27] G. D. Westfall,[23] A. Wetzler,[20] C. Whitten, Jr.,[7] H. Wieman,[20] S. W. Wissink,[16] R. Witt,[47] J. Wood,[7] J. Wu,[35] N. Xu,[20] Z. Xu,[35] Z. Xu,[3] E. Yamamoto,[20] P. Yepes,[33] V. I. Yurevich,[11] Y. V. Zanevsky,[11] H. Zhang,[3] W. M. Zhang,[19] Z. P. Zhang,[35] P. A. Zolnierczuk,[16] R. Zoulkarneev,[12] Y. Zoulkarneeva,[12] and A. N. Zubarev[11]

(STAR Collaboration*)

[1]*Argonne National Laboratory, Argonne, Illinois 60439, USA*
[2]*University of Birmingham, Birmingham, United Kingdom*
[3]*Brookhaven National Laboratory, Upton, New York 11973, USA*
[4]*California Institute of Technology, Pasedena, California 91125, USA*
[5]*University of California, Berkeley, California 94720, USA*

[6]*University of California, Davis, California 95616, USA*
[7]*University of California, Los Angeles, California 90095, USA*
[8]*Carnegie Mellon University, Pittsburgh, Pennsylvania 15213, USA*
[9]*Creighton University, Omaha, Nebraska 68178, USA*
[10]*Nuclear Physics Institute AS CR, 250 68 Řež/Prague, Czech Republic*
[11]*Laboratory for High Energy (JINR), Dubna, Russia*
[12]*Particle Physics Laboratory (JINR), Dubna, Russia*
[13]*University of Frankfurt, Frankfurt, Germany*
[14]*Institute of Physics, Bhubaneswar 751005, India*
[15]*Indian Institute of Technology, Mumbai, India*
[16]*Indiana University, Bloomington, Indiana 47408, USA*
[17]*Institut de Recherches Subatomiques, Strasbourg, France*
[18]*University of Jammu, Jammu 180001, India*
[19]*Kent State University, Kent, Ohio 44242, USA*
[20]*Lawrence Berkeley National Laboratory, Berkeley, California 94720, USA*
[21]*Massachusetts Institute of Technology, Cambridge, Massachusetts 02139-4307, USA*
[22]*Max-Planck-Institut für Physik, Munich, Germany*
[23]*Michigan State University, East Lansing, Michigan 48824, USA*
[24]*Moscow Engineering Physics Institute, Moscow, Russia*
[25]*City College of New York, New York City, New York 10031, USA*
[26]*NIKHEF, Amsterdam, The Netherlands*
[27]*Ohio State University, Columbus, Ohio 43210, USA*
[28]*Panjab University, Chandigarh 160014, India*
[29]*Pennsylvania State University, University Park, Pennsylvania 16802, USA*
[30]*Institute of High Energy Physics, Protvino, Russia*
[31]*Purdue University, West Lafayette, Indiana 47907, USA*
[32]*University of Rajasthan, Jaipur 302004, India*
[33]*Rice University, Houston, Texas 77251, USA*
[34]*Universidade de Sao Paulo, Sao Paulo, Brazil*
[35]*University of Science & Technology of China, Anhui 230027, China*
[36]*Shanghai Institute of Applied Physics, Shanghai 201800, China*
[37]*SUBATECH, Nantes, France*
[38]*Texas A&M University, College Station, Texas 77843, USA*
[39]*University of Texas, Austin, Texas 78712, USA*
[40]*Tsinghua University, Beijing 100084, China*
[41]*Valparaiso University, Valparaiso, Indiana 46383, USA*
[42]*Variable Energy Cyclotron Centre, Kolkata 700064, India*
[43]*Warsaw University of Technology, Warsaw, Poland*
[44]*University of Washington, Seattle, Washington 98195, USA*
[45]*Wayne State University, Detroit, Michigan 48201, USA*
[46]*Institute of Particle Physics, CCNU (HZNU), Wuhan 430079, China*
[47]*Yale University, New Haven, Connecticut 06520, USA*
[48]*University of Zagreb, Zagreb, HR-10002, Croatia*
(Received 15 April 2004; published 6 October 2004)

We present STAR measurements of charged hadron production as a function of centrality in Au+Au collisions at $\sqrt{s_{NN}}=130$ GeV. The measurements cover a phase space region of $0.2<p_T<6.0$ GeV/c in transverse momentum and $-1<\eta<1$ in pseudorapidity. Inclusive transverse momentum distributions of charged hadrons in the pseudorapidity region $0.5<|\eta|<1$ are reported and compared to our previously published results for $|\eta|<0.5$. No significant difference is seen for inclusive p_T distributions of charged hadrons in these two pseudorapidity bins. We measured $dN/d\eta$ distributions and truncated mean p_T in a region of $p_T>p_T^{\mathrm{cut}}$, and studied the results in the framework of participant and binary scaling. No clear evidence is observed for participant scaling of charged hadron yield in the measured p_T region. The relative importance of hard scattering processes is investigated through binary scaling fraction of particle production.

DOI: 10.1103/PhysRevC.70.044901 PACS number(s): 25.75.Dw

*URL: www.star.bnl.gov

I. INTRODUCTION

Quantum chromodynamics (QCD) is considered to be the underlying theory of the strong interaction which governs hadron production in nuclear collisions. The strong interaction is usually divided into soft processes, which involve small momentum transfer, and hard processes, which can be calculated using perturbative QCD. The Relativistic Heavy Ion Collider (RHIC) experiments at the Brookhaven National Laboratory investigate the properties and evolution of matter at high temperature and energy density. At RHIC energies, the hard processes become more evident in comparison to previous heavy ion experiments and can be used to probe the early state of the collision system. A high energy parton produced via hard scattering may lose energy in the hot/dense medium through gluon bremsstrahlung and multiple scatterings before hadronization [1,2], leading to a suppression of high p_T hadron production. The magnitude of the energy loss provides an indirect signature of QGP formation. Since parton energy loss is directly proportional to gluon density, the energy loss would be much larger in a partonic medium than in hadronic matter [3].

Partonic energy loss can be investigated through comparison of hadron yield as a function of p_T between nucleus-nucleus collisions and $p+p$ or $\bar{p}+p$ collisions. In order to do so, scaling factors which account for the nuclear geometry, the number of participant nucleons, N_{part}, and the number of binary nucleon-nucleon collisions, N_{bin}, are calculated from theoretical models. Experimental results from the RHIC, including our earlier analyses in the pseudorapidity region $|\eta|<0.5$, have indicated a suppression of hadron production for $p_T>2$ GeV/c in central Au+Au collisions relative to $p+p$ and $\bar{p}+p$ collisions [4–6]. This is in contrast to the SPS result from central Pb+Pb collisions at $\sqrt{s_{NN}}=17$ GeV, which shows an excess of π^0 production for $2<p_T<4$ GeV/c [7,8]. The RHIC measurements are striking considering that known nuclear effects, like the Cronin effect [9] and radial flow [10], tend to enhance hadron yields at high p_T. The RHIC results for high p_T hadron suppression agree qualitatively with calculations based on fragmentation models, which attribute the high p_T hadron suppression to medium induced parton energy loss [11].

Another known nuclear effect, nuclear shadowing, also modifies particle production at high p_T. Calculations of this effect [12] based on the EKS98 shadowing parametrization [13] predicted it to be small in the p_T and pseudorapidity region covered in this measurement. However, another study [14] found a much larger shadowing effect for heavy nuclei at the RHIC. Therefore, a measurement of particle production as a function of p_T and pseudorapidity may provide a constraint on the shadowing effect.

Partonic energy loss may also be studied by the pseudorapidity dependence of hadron production. The change of pseudorapidity due to change of momentum is

$$\delta\eta = \frac{p_z}{p}\left(\frac{\delta p_z}{p_z} - \frac{\delta p_T}{p_T}\right). \tag{1}$$

The pseudorapidity distributions will be modified as a result of the parton energy loss if the momentum change rate ($\delta p/p$) due to the energy loss is different along the transverse and longitudinal directions. In addition, Polleri and Yuan [15] pointed out that the degree of the energy loss may also depend on the pseudorapidity region in which a jet is produced because the energy loss is proportional to the particle density in pseudorapidity. The pseudorapidity dependence of high p_T hadron production provides a means to probe the initial density of matter along both the transverse and longitudinal directions.

In this article, we present measurements of hadron production in Au+Au collisions at $\sqrt{s_{NN}}=130$ GeV as a function of centrality, p_T, and η. In Sec. II we will briefly describe the STAR experimental setup and then give a description of data analysis techniques that were used to obtain the inclusive transverse momentum distributions for charged hadrons. We will also discuss the parametrization of inclusive transverse momentum distributions in $p+p$ collisions at $\sqrt{s}=130$ GeV and the calculations of N_{part} and N_{bin}. In Sec. III results from the data analysis will be reported and compared with model calculations. The physics implications of our measurements are discussed in Sec. IV, and we will then summarize our measurements in Sec. V.

II. ANALYSIS

A. Experimental setup and data

Measurements presented in this article are based on two data sets of Au+Au collisions at $\sqrt{s_{NN}}=130$ GeV, which were recorded by the STAR detector at the RHIC. A detailed description of the STAR detector can be found elsewhere [16]. The two data sets comprise minimum bias and central collision triggered events which correspond to approximately the most central 10% of the Au+Au geometric cross section. Charged particle tracks of an event were detected in the time projection chamber [17] (TPC) with a pseudorapidity coverage $|\eta|<1.8$ and complete azimuthal symmetry. The transverse momentum of a track is determined by fitting a circle through the transverse coordinates of the primary event vertex and the space points along the track in the TPC. The total momentum can be calculated using this radius of curvature in a 0.25 T magnetic field and the polar angle of the track. The procedure involves a three-dimensional fit using three coordinates of the primary vertex determined from all of the tracks reconstructed in the TPC. The primary vertex position along the beam direction, z_{vtx}, has a wide spread with one standard deviation about 100 cm. To increase detection efficiency of the tracks within $|\eta|<1$, we required the events to have a primary vertex $|z_{\mathrm{vtx}}|<75$ cm. After the event selection cuts, the minimum bias data set contained $\sim$181 k events and the central data set contained $\sim$365 k events.

Centrality selection is based on the uncorrected primary charged particle multiplicity N_{ch} within $|\eta|<0.75$ and $p_T<1.5$ GeV/c. The requirement on the η range maximizes the number of tracks used to define centrality in an event while keeping the tracking acceptance approximately constant. The percentage of the geometric cross section is determined in the same way as that published by STAR previously [18], where the negatively charged hadron multiplicity N_{h^-} distribution within $|\eta|<0.5$ was used. The data set is

TABLE I. Typical multiplicative correction factors and systematic uncertainties, applied to the yields for peripheral and central collisions within $|\eta|<0.5$ and within $0.5<|\eta|<1$.

		p_T=2 GeV/c		p_T=5.5 GeV/c	
Pseudorapidity	Centrality	(60–80)%	(0–5)%	(60–80)%	(0–5)%
$\|\eta\|<0.5$	Tracking	1.16±0.10	1.71±0.15	1.22±0.16	1.65±0.22
	p_T smearing	1.01±0.01	1.00±0.01	0.89±0.02	0.70±0.06
	Background	0.92±0.04	0.88±0.06	0.90±0.10	0.85±0.15
$0.5<\|\eta\|<1$	Tracking	1.29±0.11	1.78±0.15	1.31±0.18	1.71±0.23
	p_T smearing	1.01±0.01	1.01±0.01	0.89±0.02	0.72±0.07
	Background	0.92±0.04	0.88±0.06	0.96±0.04	0.94±0.06

divided into seven centrality bins, and the most central bin is (0–5)% (the top 5% of the multiplicity distribution) while the most peripheral bin is (60–80)%.

The analysis in this article covers a transverse momentum region of $0.2<p_T<6.0$ GeV/c. Accepted primary tracks have $|\eta|<1$, at least 25 space points in the TPC used in the track fit out of 45 pad rows, a fit probability of being a primary track greater than 0.05, and a distance of closest approach to the primary vertex less than 1 cm. These track quality cuts were varied to estimate the systematic uncertainty. Acceptance and efficiency were determined by embedding simulated tracks into actual Au+Au collision events.

The measured high p_T hadron yield is sensitive to small spatial distortions of the TPC alignments in both azimuthal and longitudinal directions. A measurement of the summed hadron yield $(h^++h^-)/2$ is less sensitive to such distortions than the yield of one charge sign alone. We call such distortion the charge-sign-dependent distortion. Using 12 sectors from each of the TPC ends as independent detectors for high p_T hadrons, we estimated the sectorwise (azimuthal direction) variations of the yields to be less than 5%. The variation of the yield between the hadrons crossing and not crossing the central membrane of the TPC was found to be approximately proportional to p_T with a value of 11% at p_T =5.5 GeV/c. The typical correction factors for the acceptance and efficiency are given in Table I as "Tracking." The systematic uncertainties incorporate acceptance, efficiency, track quality cuts, and the effects of the spatial nonuniformity. The tracking and other correction factors and their systematic uncertainties given in Table I for $|\eta|<0.5$ differ from those given in our previous paper [4] because different track quality cuts and other correction procedures were used.

Finite momentum resolution tends to spread particles to neighboring bins in a momentum histogram, especially for an exponentially falling spectrum. This smearing effect cannot be neglected at higher p_T where the momentum resolution is limited by the strength of the magnetic field and the TPC spatial resolution. We used the embedding technique to determine the p_T resolution. For $p_T>0.5$ GeV/c within $|\eta|<0.5$ the Gaussian distribution of track curvature $k \propto 1/p_T$ has a relative width of $\delta k/k=0.013+0.015p_T/(\mathrm{GeV}/c)$ for central events and $\delta k/k=0.012+0.012p_T/(\mathrm{GeV}/c)$ for peripheral events. Within $0.5<|\eta|<1$, $\delta k/k=0.014+0.010p_T/(\mathrm{GeV}/c)$ for central events and $\delta k/k=0.014+0.0072p_T/(\mathrm{GeV}/c)$ for peripheral events.

The fact that the p_T resolution for $0.5<|\eta|<1$ is better than that for $|\eta|<0.5$ is due to the competition between two opposing effects. For a given p_T track in the TPC, the hadron with higher η tends to have fewer space points, hence poorer resolution, but shorter drift distance, hence better resolution.

The magnitude of the p_T resolution determined from the embedding technique did not include the effect of the primary vertex resolution. The effects of the p_T smearing due to the primary vertex resolution, to the charge-sign-dependent distortion, and to the weak decay background tracks have been empirically derived from the comparison between real and embedded tracks. The combined effect within $0.5<|\eta|<1$ was found to be larger than that within $|\eta|<0.5$. This is partially due to the fact that the magnitude of the charge-sign-dependent distortion in the higher η region is larger.

The two contributions to the p_T smearing investigated above have been convoluted into a power law function to fit the data, and then the ratio of the fitted function to its convoluted one gives the p_T smearing correction factor [19]. Because the two contributions have opposite $|\eta|$ dependence, the overall p_T smearing correction factors for the two η regions happen to be comparable. The typical p_T smearing correction factors and their systematic uncertainties are also given in Table I.

B. Background

The most significant backgrounds for the high p_T charged hadron yield as seen in Table I come from particle weak decays and antinucleon annihilation in detector material. The contamination rate for each background source was estimated using detector response simulations with events generated by the HIJING model [20]. However, the p_T dependence of production of weakly decaying particles, primarily $K^0_S, \Lambda, \overline{\Lambda}$, and of antinucleons $\overline{p}, \overline{n}$ in HIJING is not consistent with experimental measurements. We corrected those predicted yields using the measured spectra of $\overline{p}$ [21,22], Λ and $\overline{\Lambda}$ [23], and K^0_S [24], together with those of h^- [18,21], for $p_T<2.4$ GeV/c in the midrapidity region in the most central bin. The corrections used in calculating the background fractions are shown in the upper panel of Fig. 1. The curves are polynomial fits to the data points and are used in

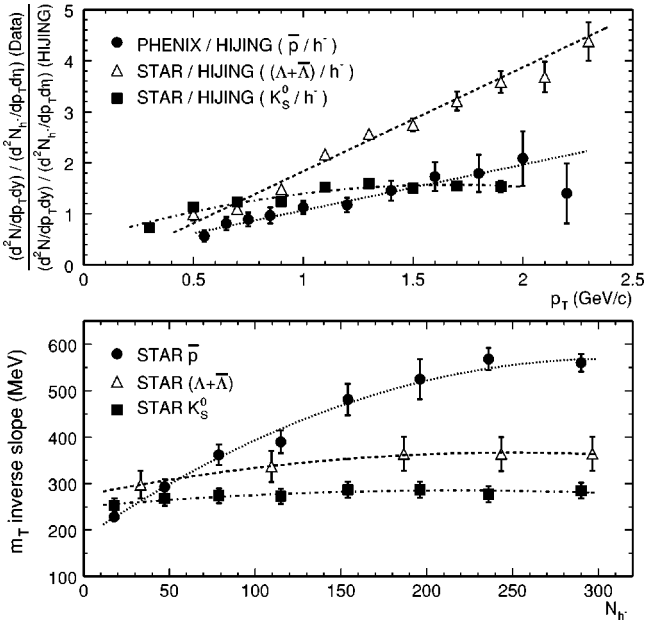

FIG. 1. Measurements used in background studies. Upper panel: ratios of the measured p_T yield ratios to those of HIJING in the most central bin. Lower panel: measured m_T inverse slope parameters as functions of centrality represented by measured negatively charged hadron multiplicity N_{h^-} within $|\eta|<0.5$. Curves are polynomial fits to data points.

the interpolation due to different p_T binning. For $p_T>2.4$ GeV/c we simply assumed the yield ratios to be constant [25]. Systematic uncertainties of 50% and 100% of the overall background fraction are assigned for the regions of $p_T<2.4$ GeV/c and $p_T>2.4$ GeV/c, respectively [19].

The contamination rate for all background sources shows almost no centrality dependence from the Monte Carlo HIJING events. Therefore, the centrality dependence of the background fraction is mainly determined by the measured spectra in various centrality bins. In the lower panel of Fig. 1 we show the measured transverse mass ($m_T=\sqrt{p_T^2+m_0^2}$) inverse slope parameters of exponential fits to $\bar{p}$ [22], Λ and $\bar{\Lambda}$ [23], and K_S^0 [24] spectra in the midrapidity region as functions of the measured negatively charged hadron multiplicity N_{h^-} within $|\eta|<0.5$. We use these to correct for different centrality binning in our analysis. The polynomial fits are used to interpolate the inverse slope parameters in the centrality bins used in this analysis.

Pseudorapidity dependence of the background fraction is studied using the Monte Carlo HIJING events. For $p_T<2$ GeV/c the η dependence of backgrounds is negligible within $-1<\eta<1$ while for $p_T>2$ GeV/c the background fraction decreases with increasing p_T and $|\eta|$. For example, at $p_T=5.5$ GeV/c the background fraction predicted within $0.5<|\eta|<1$ is only 40% of that within $|\eta|<0.5$. The typical background correction factors and their systematic uncertainties are given in Table I. The total systematic uncertainties of the measured spectra within $|\eta|<0.5$ ($0.5<|\eta|<1$) at the highest bin $p_T=5.5$ GeV/c are $\approx$24% ($\approx$18%) for central events and $\approx$17% ($\approx$15%) for peripheral events.

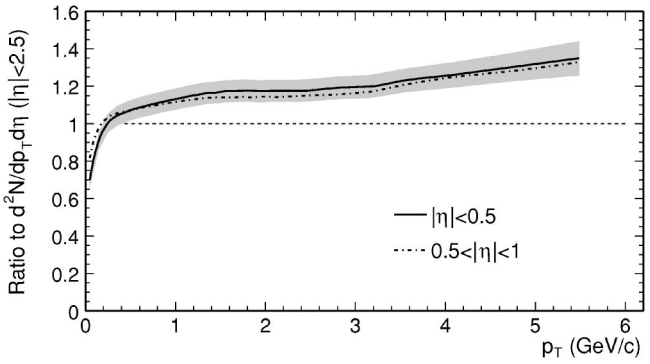

FIG. 2. η acceptance correction function from model calculations: ratios of p_T spectra in two different η regions to that within $|\eta|<2.5$, in which the UA1 Collaboration published its inclusive charged particle p_T spectra.

C. *NN* reference

In the absence of any *NN* collision data at $\sqrt{s}=130$ GeV, a *NN* reference spectrum is obtained by extrapolation of the UA1 $\bar{p}+p$ data for $\sqrt{s}=200-900$ GeV [26]. The UA1 inclusive charged particle p_T spectra within $|\eta|<2.5$ were fitted by the perturbative QCD (PQCD) inspired power law function

$$\frac{1}{2\pi p_T}\frac{d^2N}{dp_T d\eta}=C\left(1+\frac{p_T}{p_0}\right)^{-n}. \tag{2}$$

The fit parameters were used to extrapolate to our energy, giving $C\sigma_{\rm in}=267^{+4}_{-6}$ mb/(GeV/c)^2 ($\sigma_{\rm in}$ denotes the inelastic cross section of *NN* collisions), $p_0=1.90^{+0.17}_{-0.09}$ GeV/c, and $n=12.98^{+0.92}_{-0.47}$ at $\sqrt{s}=130$ GeV [4]. The superscripts and subscripts are curves that bound the systematic uncertainty.

However, the UA1 acceptance is different from STAR's. Corrections were made to the UA1 reference for our η acceptance based on two independent PQCD calculations: those of PYTHIA [27] and Vitev [28]. When the *K* factor in PYTHIA is set to 1.5, PYTHIA calculations for 200 GeV $\bar{p}+p$ collisions are in reasonable agreement with the UA1 measurement of the inclusive charged particle p_T spectrum [26] and with the UA5 measurement of the pseudorapidity density distribution [29]. Similar PYTHIA calculations are in reasonable agreement with the STAR measurement of the inclusive charged hadron p_T spectrum within $|\eta|<0.5$ for $p+p$ collisions at $\sqrt{s}=200$ GeV [5]. Figure 2 shows the p_T-dependent correction functions for two η regions at $\sqrt{s}=130$ GeV, obtained by averaging over the two PQCD calculations. The solid curve is the ratio of $d^2N/dp_T d\eta$ within $|\eta|<0.5$ to that within $|\eta|<2.5$, and the shaded area shows its systematic uncertainty. The dot-dashed curve shows the same ratio for $0.5<|\eta|<1$, and the similar magnitude of the uncertainty on the ratio of $0.5<|\eta|<1$ to $|\eta|<2.5$ is not shown. Multiplicative corrections of 1.35 ± 0.09 and 1.33 ± 0.09 at $p_T=5.5$ GeV/c have been obtained for $|\eta|<0.5$ and for $0.5<|\eta|<1$, respectively. The difference between $|\eta|<0.5$ and $0.5<|\eta|<1$ is quite small, indicating a relatively flat η distribution within $-1<\eta<1$ for a broad

TABLE II. Comparisons of nuclear geometries implemented in various models for 130 GeV Au+Au collisions.

Model	HIJING 1.35	VENUS 4.12	MC Glauber
Woods-Saxon parameters	$r_0=6.38$ fm $D=0.535$ fm	$r_0=6.64$ fm $D=0.540$ fm	$r_0=6.5\pm0.1$ fm $D=0.535\pm0.027$ fm
Minimum distance of two nucleons	0.4 fm	0.8 fm	0.4 fm
Nucleon-nucleon overlap function	$\Omega(b)=(1+\sigma_{\rm jet}/\sigma_{\rm soft})\chi_0(\xi)$ $\xi=b/b_0(s)$ $\chi_0(\xi)=\mu_0^2(\mu_0\xi)^3K_3(\mu_0\xi)/96$	$\theta(R-b)$	$\theta(R-b)$
Maximum impact parameter	25.6 fm	24.1 fm	No restriction
Nucleon-nucleon cross section $\sigma_{\rm in}$	38.7 mb	37.4 mb	41 ± 1 mb
Total geometric cross section	7.27 b	7.34 b	6.9 ± 0.4 b

p_T region. The STAR measurement [5] is consistent with the UA1 $\bar{p}+p$ data for 200 GeV after applying a similar η acceptance correction.

We derived $\sigma_{\rm in}$ in the NN reference at $\sqrt{s}=130$ GeV of 40 ± 3 mb by requiring $dN/d\eta$ ($|\eta|<0.5$), which was obtained by integrating the extrapolated spectrum after applying the η acceptance correction, to be 2.25, which was determined from the energy dependence of $dN/d\eta$ ($\eta=0$) [30].

D. Participant and binary collision determination

The number of participant nucleons, $N_{\rm part}$, and the number of binary nucleon-nucleon collisions, $N_{\rm bin}$, in a nucleus-nucleus collision are used to compare experimental results with model predictions. Unfortunately, at RHIC $N_{\rm part}$ and $N_{\rm bin}$ cannot be measured directly and have to be obtained in a model-dependent way. Considerable discrepancy exists among various model calculations, especially for peripheral collisions [31].

We first investigate $N_{\rm part}$ and $N_{\rm bin}$ obtained from a Monte Carlo (MC) Glauber model calculation [4,32]. In the Monte Carlo Glauber model, each of the nucleons in a nucleus A is randomly distributed using a Woods-Saxon nuclear density distribution

$$\rho(r)=\frac{\rho_0}{1+\exp[(r-r_0)/D]}, \tag{3}$$

with normalization to $\int\rho(r)dr=A$ and parameters nuclear radius r_0 and surface diffuseness D. All nucleons in either nucleus for a nucleus-nucleus collision are required to be separated by a minimum distance. The calculated $d\sigma/dN_{\rm part}$ or $d\sigma/dN_{\rm bin}$ distribution was divided into bins corresponding to common fractions of the total geometric cross section to extract the average $N_{\rm part}$ or $N_{\rm bin}$ for each centrality bin. The systematic uncertainties on $N_{\rm part}$ and $N_{\rm bin}$ were estimated by varying the Woods-Saxon parameters, by varying the $\sigma_{\rm in}$ value, and by including a 5% uncertainty in the determination of the total geometric cross section.

We also investigate calculations of $N_{\rm part}$ and $N_{\rm bin}$ using two dynamic models, HIJING [20] and VENUS [33]. We compare these calculations with results from the Monte Carlo Glauber model calculation to shed light on the model-dependent uncertainties of $N_{\rm part}$ and $N_{\rm bin}$.

The VENUS model is based on the Gribov-Regge theory and string fragmentation. The HIJING generator is an example of a two-component model: the momentum transfer of the soft process is treated phenomenologically and the hard processes are calculated by PQCD. The excited nucleons after collisions are stretched out as quark-diquark strings and fragments based on the Lund fragmentation scheme [34]. The parton energy loss in a dense medium (quenching) and nuclear modification of parton structure functions (shadowing) are also modeled in HIJING.

Both dynamic models describe nuclear collision geometry using the Woods-Saxon nuclear density distribution and the eikonal formalism to determine the probability for each binary nucleon-nucleon collision, and to compute $N_{\rm part}$ and $N_{\rm bin}$. Table II shows the comparisons of the nuclear geometries implemented in HIJING, VENUS, and the Monte Carlo Glauber model for Au+Au collisions at $\sqrt{s_{NN}}=130$ GeV. The overlap function, which defines the probability for a nucleon-nucleon collision at a given impact parameter b, has the form of $1-\exp[-2\Omega(b)]$ in HIJING with $\Omega(b)$ defined in Table II [$\mu_0=3.9$ and $\pi b_0^2(s)=\sigma_{\rm soft}(s)/2$] while it is a step function $\theta(R-b)$ in VENUS and MC Glauber.

The correspondence between the centrality classes defined by measured charged particle multiplicity and those defined by modeled impact parameter was used to extract the average $N_{\rm part}$ and $N_{\rm bin}$ from these dynamic models for a given centrality bin. Variations of average $N_{\rm part}$ and $N_{\rm bin}$ for different centrality selections were estimated using the Monte Carlo events from the HIJING model. The event classes corresponding to the same fractional cross section were selected by cuts on $b, N_{\rm ch}, N_{\rm part}$, and $N_{\rm bin}$. The average $N_{\rm part}$ and $N_{\rm bin}$ by different cuts in HIJING are consistent within 2% for each centrality bin except the (60–80)% most peripheral bin, where the discrepancy is at a level of 6%.

The results of $N_{\rm part}$ and $N_{\rm bin}$ from the models are shown in Fig. 3 as their ratios to $N_{\rm part}$ or $N_{\rm bin}$ from the Monte Carlo Glauber calculation. The participant scaling exponents α,

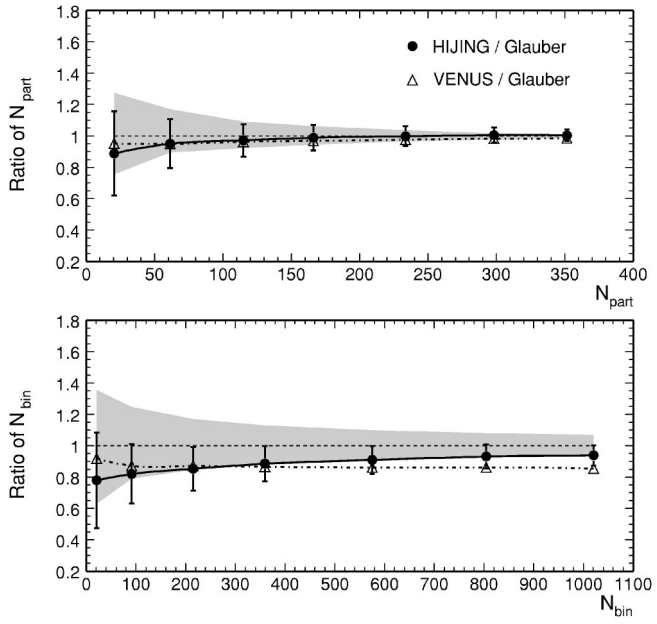

FIG. 3. Ratio of the number of participants, N_{part} (upper panel), or the number of binary collisions, N_{bin} (lower panel), determined from different models to that from a Monte Carlo Glauber calculation. Shaded areas show the uncertainties of N_{part} or N_{bin} from the Monte Carlo Glauber calculation. Curves are to guide the eye.

which are defined in the expression of $N_{\text{bin}}=B\cdot N_{\text{part}}^{\alpha}$, were obtained by fit to be $1.41\pm0.08, 1.34\pm0.08$, and 1.38 ± 0.08 for HIJING, VENUS, and MC Glauber. The scaling exponents α for these models are approximately $4/3$ due to the fact that $N_{\text{part}}\propto A^1$ and $N_{\text{bin}}\propto A^{4/3}$.

It is worthwhile to note here that distribution differences among HIJING and VENUS are mainly due to different overlap functions. The N_{part} and N_{bin} distributions from them are nearly identical if the same overlap functions are used in these two model calculations. Figure 3 shows that over a broad range of centrality the model-dependent uncertainties of N_{part} and N_{bin} are within 10% and 20%, respectively.

III. RESULTS

Inclusive p_T distributions of $(h^++h^-)/2$ within $|\eta|<0.5$ have been published previously [4]. The independent analysis reported in this article shows that the differences from the published results for all measured p_T points are within 10%, which is comparable to the systematic uncertainties for $p_T<2$ GeV/c and is less than the systematic uncertainties for the high p_T region. Figure 4 shows inclusive p_T distributions of $(h^++h^-)/2$ within $0.5<|\eta|<1$ for various centrality bins. The error bars are the quadrature sum of statistical error and systematic uncertainty, and are dominated by the latter except for the highest p_T point in the peripheral bins. The curves in Fig. 4 are power law function [Eq. (2)] fits to the spectra.

Figure 5 shows ratios of p_T distributions within $0.5<|\eta|<1$ to those within $|\eta|<0.5$ in various centrality bins. Note that Fig. 5 and the succeeding figures utilize the p_T distributions within $|\eta|<0.5$ obtained here. Using identical cuts and correction procedures across the full pseudorapidity region minimizes the systematic uncertainties in the relative comparisons. The error bars in Fig. 5 show statistical errors only while the caps are the quadrature sum of statistical errors and systematic uncertainties which cannot be canceled out. Remaining systematic uncertainty includes the variation due to track quality cuts, the uncertainties of the p_T smearing corrections for the two η regions, and the partial uncertainty of background subtraction related to the η-dependent part discussed in Sec. II.

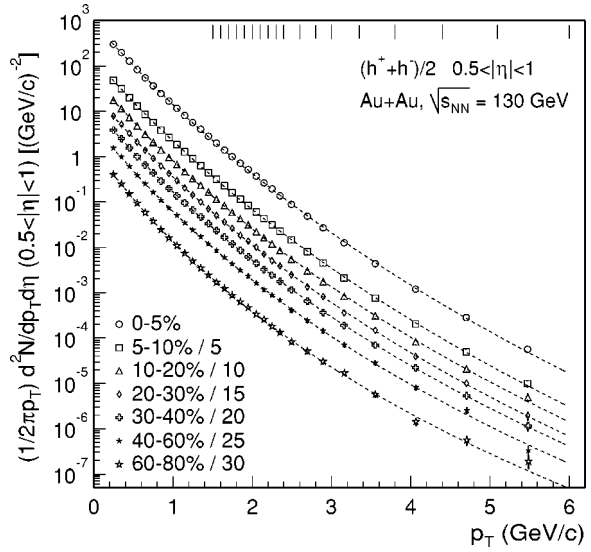

FIG. 4. Inclusive p_T distributions of $(h^++h^-)/2$ within $0.5<|\eta|<1$. Noncentral bins are scaled down by the indicated factors. The combined statistical and systematic errors are shown. Curves are fits to the power law function. Tick marks at the top indicate bin boundaries for $p_T>1.5$ GeV/c.

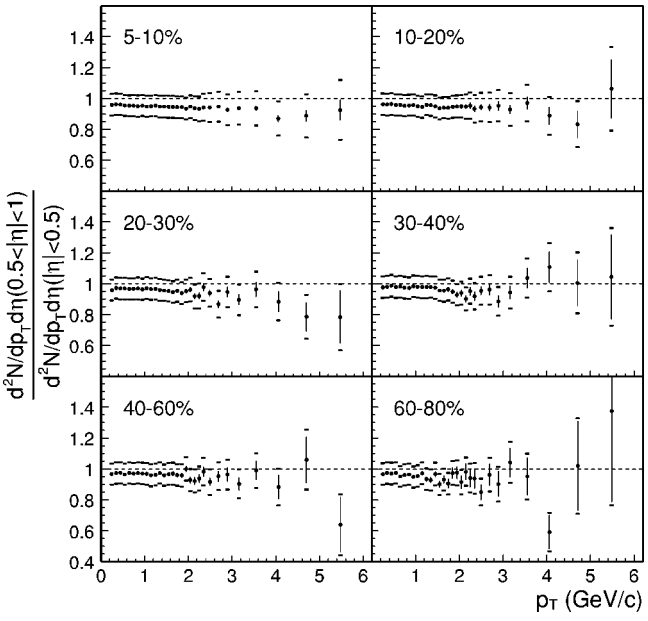

FIG. 5. Ratios of p_T distributions within $0.5<|\eta|<1$ to those within $|\eta|<0.5$ in various centrality bins. Error bars show statistical errors while caps are the quadrature sum of statistical errors and remaining systematic uncertainties.

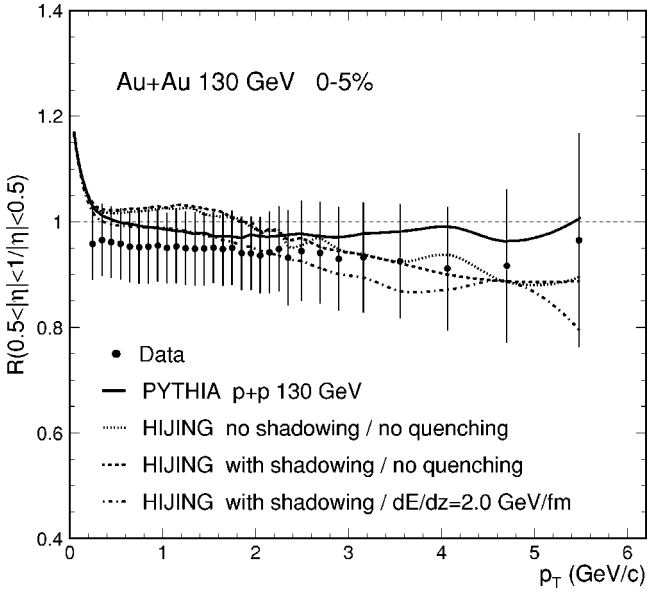

FIG. 6. Ratio of p_T distribution within $0.5<|\eta|<1$ to that within $|\eta|<0.5$ in the 0–5% most central bin. Points are measurements and error bars include statistical and remaining systematic uncertainties. Curves are described in the text.

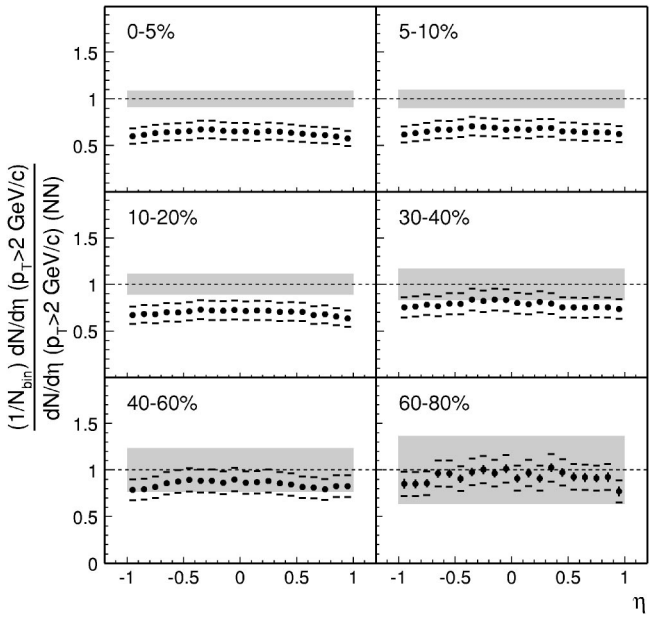

FIG. 7. $dN/d\eta$ distributions for $p_T>2$ GeV/c and $-1<\eta<1$ scaled by $N_{\rm bin}$ and divided by the *NN* reference.

Figure 6 shows the same ratio of $0.5<|\eta|<1$ to $|\eta|<0.5$ in the (0–5)% most central bin. The points are our measurements and the error bars include statistical and remaining systematic uncertainties. The solid curve is the same ratio from PYTHIA calculations [27] for 130 GeV $p+p$ collisions. Other curves are ratios from HIJING predictions of 130 GeV Au+Au collisions without shadowing and without quenching (dotted curve), with shadowing and without quenching (dashed curve), and with shadowing and with partonic energy loss being 2.0 GeV/fm (dot-dashed curve). The results show that the effects on the pseudorapidity dependence of both nuclear shadowing and partonic energy loss as implemented in HIJING are too small to be tested in the measured kinematic region under current experimental uncertainties.

No significant differences are observed in the comparisons of the inclusive charged hadron yields between the two η regions in Fig. 5 and Fig. 6 over a broad range of centrality for all measured p_T points. It suggests that an approximate boost invariant condition might be established in the early stage of collisions. The suppression pattern of the particle yield has little η dependence in the measured region though the particle yield itself is sensitive to partonic energy loss. A measurement of this ratio between $\eta=2.2$ and $\eta=0$ from the BRAHMS Collaboration shows that the ratio is below unity at $p_T\sim 4$ GeV/c [35].

Figure 7 shows $dN/d\eta$ distributions for $p_T>2$ GeV/c and $-1<\eta<1$ in various centrality bins. The error bars show statistical uncertainties while the caps are the quadrature sum of statistical and systematic uncertainties. The systematic uncertainties are dominant and highly correlated. The $dN/d\eta$ distributions are scaled by $N_{\rm bin}$ and divided by the *NN* reference. Due to nearly complete η independence of the *NN* reference data for $p_T>0.2$ GeV/c within $-1<\eta<1$ as shown in Fig. 2 and Fig. 6, constant $dN/d\eta$ values of the *NN* reference are used in Fig. 7. Therefore, the shapes of the $dN/d\eta$ distributions for the Au+Au collisions are preserved. The uncertainties on both $N_{\rm bin}$ and the *NN* reference data are shown in the shaded regions around the lines at unity which represent the binary collision scaling. Ratios below unity in the figure show that the high p_T hadrons over 2 GeV/c are suppressed with respect to those in $p+p$ collisions. The shape of $dN/d\eta$ for the high p_T hadrons is nearly flat. No significant centrality dependence of the $dN/d\eta$ shapes within $-1<\eta<1$ is observed. Similar behaviors are observed for $p_T>4$ GeV/c except larger suppressions in the central bins. For example, in the (0–5)% most central bin, the average ratio is 0.41 ± 0.10 for $p_T>4$ GeV/c while it is 0.64 ± 0.10 for $p_T>2$ GeV/c.

IV. DISCUSSION

The charged hadron yield per participant pair at $\sqrt{s_{NN}}=130$ GeV shows a slow increase as a function of $N_{\rm part}$ [4,36,37]. Such a slow increase of hadron multiplicity as a function of centrality at the RHIC has been considered by Kharzeev *et al.* [38] in the framework of parton saturation. They argued that the hadron multiplicity as a function of centrality would increase faster if the produced jets lose energy, radiating soft gluons that in turn fragment into hadrons at midrapidity. As a result of the parton saturation, it is predicted that hadron multiplicity should scale with $N_{\rm part}$ at a moderately high p_T (up to 6–8 GeV/c at RHIC energies). An explanation of the slower than expected increase in fragmentation models is that the effective energy loss is significantly reduced in a thermal environment due to detailed balance [8]. Recent experimental results in $d+$Au collisions at $\sqrt{s_{NN}}=200$ GeV support the idea that the suppression of high p_T hadron production in Au+Au collisions at midrapidity is due to final state interactions rather than parton saturation in the initial state [35,39].

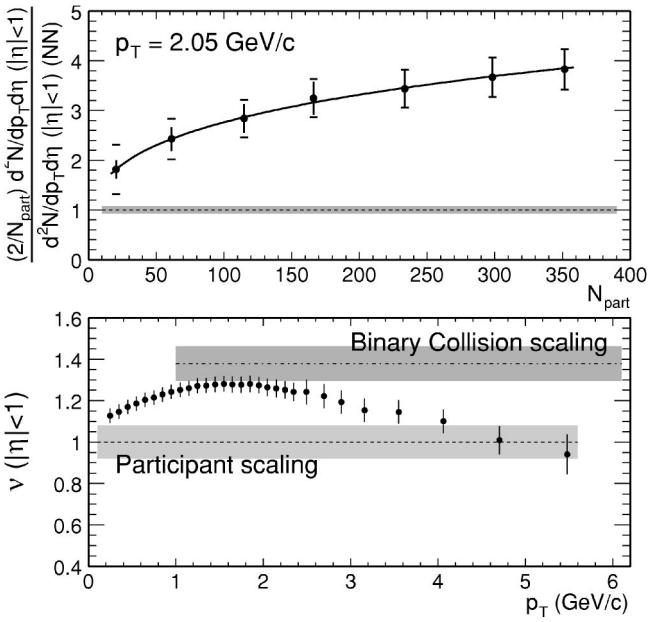

FIG. 8. Upper panel: ratio of charged hadron yields within $|\eta|<1$ for Au+Au relative to the *NN* reference, scaled by $N_{\mathrm{part}}/2$ as a function of centrality for a p_T bin at $p_T=2.05$ GeV/c. The curve is fitted to $B\cdot N_{\mathrm{part}}^{\nu}$. Lower panel: participant scaling exponent ν of charged hadron yields as a function of p_T within $|\eta|<1$.

In the upper panel of Fig. 8, we plot charged hadron yield per participant pair within $|\eta|<1$ normalized to that of nucleon-nucleon collisions as a function of N_{part} for $p_T=2.05$ GeV/c. The error bars are the uncertainties of data while the caps are the quadrature sum of the uncertainties of both data and N_{part}. The shaded regions around unity show systematic uncertainties of the *NN* reference data. The result shows that the ratio is above unity and increases with N_{part}.

Dependence of the charged hadron yield on N_{part} can be studied by fitting the yield by the following function:

$$\frac{d^2N}{dp_T d\eta} = B\cdot N_{\mathrm{part}}^{\nu} \tag{4}$$

in different p_T bins. Such an example is shown as a curve in the upper panel of Fig. 8 for $p_T=2.05$ GeV/c. The fit parameter $\nu(p_T)$ is given in the lower panel of Fig. 8 as a function of p_T. The error bars are the uncertainties of the fit parameters associated with the uncertainties of data. The lines and shaded regions are binary collision (N_{bin}) and participant (N_{part}) scaling exponents and uncertainties to N_{part}. No clear evidence of participant scaling over the whole measured p_T region is observed. The approximate participant scaling of the hadron yield at high p_T observed by PHOBOS [40] appears to be accidental.

In a scenario with continuous energy loss of particles through a medium, the energy loss would lead to a shift in the mean p_T of these particles. If the energy loss contributes to additional particle production in the low p_T region, the mean p_T of low p_T particles will also be modified. The truncated mean p_T, defined as

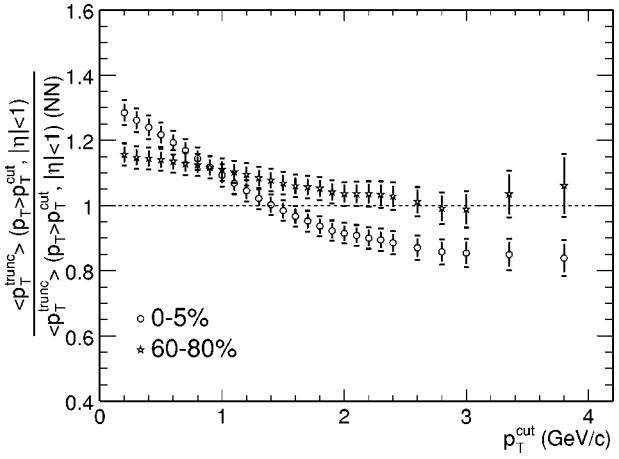

FIG. 9. Ratio of truncated mean p_T in $p_T>p_T^{\mathrm{cut}}$ within $|\eta|<1$ as a function of p_T^{cut} for central and peripheral collisions.

$$\langle p_T^{\mathrm{trunc}}\rangle(p_T^{\mathrm{cut}}) = \frac{\int_{p_T^{\mathrm{cut}}}^{\infty} p_T\cdot dN/dp_T\cdot dp_T}{\int_{p_T^{\mathrm{cut}}}^{\infty} dN/dp_T\cdot dp_T} - p_T^{\mathrm{cut}}, \tag{5}$$

is used to study the variation of mean p_T as a function of p_T scale with respect to *NN* reference data. Figure 9 shows the truncated mean p_T ratios between Au+Au and $p+p$ collisions as a function of p_T^{cut} for central [(0–5)%] and peripheral [(60–80)%] collisions. The errors are combined statistical and systematic uncertainties while the caps are the quadrature sum of the uncertainties of both the Au+Au data and the *NN* reference data.

In peripheral collisions at high p_T ($p_T^{\mathrm{cut}}\gtrsim 3$ GeV/c) the truncated mean p_T of particles is approximately the same as for $p+p$ collisions above the same p_T^{cut} (Fig. 9). The ratio in the low p_T region is above unity indicating the effects of the Cronin effect and/or radial flow in peripheral collisions. For central collisions, the truncated mean p_T for $p_T^{\mathrm{cut}}\gtrsim 3$ GeV/c is approximately 15% lower than the truncated mean p_T from $p+p$ collisions at the same p_T^{cut}, consistent with the scenario for partonic energy loss in this p_T region. The significantly larger ratio in the low p_T region probably reflects the combined effects of larger radial flow, the Cronin effect, and p_T shift of particles due to energy loss, which cannot be decoupled with the present data.

Figure 8 (bottom panel) indicates that over a broad p_T region particle production falls between participant and binary scalings. In two-component particle production models, the binary scaling has been associated with hard parton scatterings and the participant scaling with the soft processes. In our study we empirically decompose the particle yield into N_{part} and N_{bin} scaling components, i.e.,

$$dN/d\eta(p_T^{\mathrm{cut}}) = \left[1-x(p_T^{\mathrm{cut}})\right] n_{pp}(p_T^{\mathrm{cut}})\cdot\frac{N_{\mathrm{part}}}{2} + x(p_T^{\mathrm{cut}})\, n_{pp}(p_T^{\mathrm{cut}})\cdot N_{\mathrm{bin}}, \tag{6}$$

where $n_{pp}(p_T^{\mathrm{cut}})$ and $x(p_T^{\mathrm{cut}})$ are the hadron multiplicity and the fraction of particle yield attributable to hard processes in $p+p$ collisions, respectively. Figure 10 shows the binary

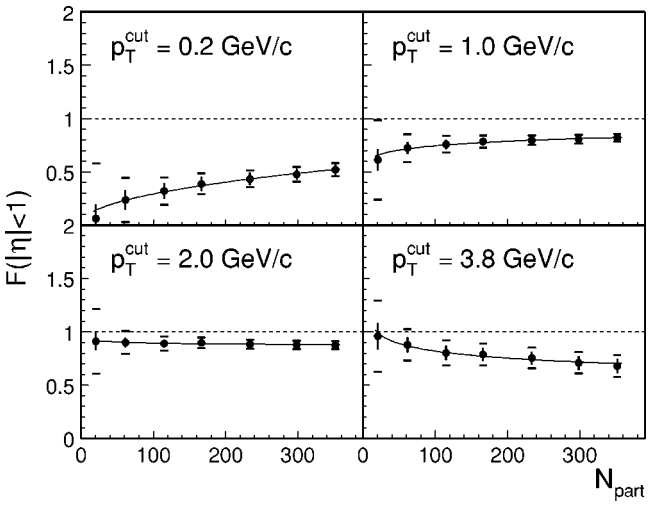

FIG. 10. Binary scaling fraction in $p_T > p_T^{\mathrm{cut}}$ within $|\eta| < 1$ as a function of centrality for selected p_T^{cut}. For $p_T^{\mathrm{cut}} > 2$ GeV/c, the fraction F decreases with increasing centrality.

scaling fraction in Au+Au collisions, defined as

$$F(p_T^{\mathrm{cut}}) = \frac{x(p_T^{\mathrm{cut}}) n_{pp}(p_T^{\mathrm{cut}}) \cdot N_{\mathrm{bin}}}{dN/d\eta(p_T^{\mathrm{cut}})}. \quad (7)$$

Note that $F(p_T^{\mathrm{cut}})$ does not depend on $n_{pp}(p_T^{\mathrm{cut}})$ since both numerator and denominator of Eq. (7) contain $n_{pp}(p_T^{\mathrm{cut}})$. There is a distinguishable trend as a function of N_{part} from $p_T^{\mathrm{cut}} = 3.8$ GeV/c to lower p_T^{cut}. This trend is consistent with the $\nu(p_T)$ dependence in Fig. 8. It is worth noting that $F \approx 70\%$ in central Au+Au collisions at $p_T^{\mathrm{cut}} = 3.8$ GeV/c. However, one should exercise caution when relating this fraction to hard parton scattering processes, particularly at lower p_T where high p_T particles may suffer large energy losses in the medium and become soft.

V. CONCLUSION

We have presented inclusive distributions of $(h^+ + h^-)/2$ from STAR at the RHIC in the region $0.5 < |\eta| < 1$ and compared them to distributions for $|\eta| < 0.5$, finding no significant differences in the region of $0.2 < p_T < 6.0$ GeV/c. We find that the $dN/d\eta$ distributions for $-1 < \eta < 1$ are nearly flat for all centralities. The charged hadron yield as a function of p_T shows no clear participant scaling in the measured p_T region. The binary scaling fraction in the two-component model shows a decrease with centrality for $p_T^{\mathrm{cut}} > 2$ GeV/c and is about 70% at $p_T^{\mathrm{cut}} = 3.8$ GeV/c for central collisions.

ACKNOWLEDGMENTS

We thank the RHIC Operations Group and RCF at BNL, and the NERSC Center at LBNL for their support. This work was supported in part by the HENP Divisions of the Office of Science of the U.S. DOE; the U.S. NSF; the BMBF of Germany; IN2P3, RA, RPL, and EMN of France; EPSRC of the United Kingdom; FAPESP of Brazil; the Russian Ministry of Science and Technology; the Ministry of Education and the NNSFC of China; SFOM of the Czech Republic; FOM and UU of the Netherlands; DAE, DST, and CSIR of the Government of India; and the Swiss NSF.

[1] M. Gyulassy and M. Plümer, Phys. Lett. B **243**, 432 (1990); R. Baier *et al.*, *ibid.* **345**, 277 (1995).
[2] X. N. Wang and M. Gyulassy, Phys. Rev. Lett. **68**, 1480 (1992); X. N. Wang, Phys. Rev. C **58**, 2321 (1998).
[3] R. Baier, D. Schiff, and B. G. Zakharov, Annu. Rev. Nucl. Part. Sci. **50**, 37 (2000); E. Wang and X. N. Wang, Phys. Rev. Lett. **89**, 162301 (2002).
[4] STAR Collaboration, C. Adler *et al.*, Phys. Rev. Lett. **89**, 202301 (2002).
[5] STAR Collaboration, J. Adams *et al.*, Phys. Rev. Lett. **91**, 172302 (2003).
[6] PHENIX Collaboration, K. Adcox *et al.*, Phys. Rev. Lett. **88**, 022301 (2002); PHENIX Collaboration, S. S. Adler *et al.*, *ibid.* **91**, 072301 (2003).
[7] WA98 Collaboration, M. M. Aggarwal *et al.*, Phys. Rev. Lett. **81**, 4087 (1998); **84**, 578(E) (2000).
[8] E. Wang and X. N. Wang, Phys. Rev. Lett. **87**, 142301 (2001).
[9] J. W. Cronin *et al.*, Phys. Rev. D **11**, 3105 (1975).
[10] NA49 Collaboration, G. Roland, Nucl. Phys. **A638**, 91c (1998).
[11] X. N. Wang, Phys. Rev. C **61**, 064910 (2000); P. Levai *et al.*, Nucl. Phys. **A698**, 631c (2002).
[12] S. R. Klein and R. Vogt, Phys. Rev. C **67**, 047901 (2003).
[13] K. J. Eskola, V. J. Kolhinen, and P. V. Ruuskanen, Nucl. Phys. **B535**, 351 (1998); K. J. Eskola, V. J. Kolhinen, and C. A. Salgado, Eur. Phys. J. C **9**, 61 (1999).
[14] S. Y. Li and X. N. Wang, Phys. Lett. B **527**, 85 (2002).
[15] A. Polleri and F. Yuan, nucl-th/0108056; F. Yuan (private communication).
[16] STAR Collaboration, K. H. Ackermann *et al.*, Nucl. Instrum. Methods Phys. Res. A **499**, 624 (2003).
[17] STAR Collaboration, K. H. Ackermann *et al.*, Nucl. Phys. **A661**, 681c (1999); M. Anderson *et al.*, Nucl. Instrum. Methods Phys. Res. A **499**, 659 (2003).
[18] STAR Collaboration, C. Adler *et al.*, Phys. Rev. Lett. **87**, 112303 (2001).
[19] Y. Chen, Ph.D. dissertation, University of California, Los Angeles, 2003.
[20] M. Gyulassy and X. N. Wang, Comput. Phys. Commun. **83**, 307 (1994).
[21] PHENIX Collaboration, K. Adcox *et al.*, Phys. Rev. Lett. **88**, 242301 (2002).
[22] STAR Collaboration, C. Adler *et al.*, Phys. Rev. Lett. **87**, 262302 (2001).
[23] STAR Collaboration, C. Adler *et al.*, Phys. Rev. Lett. **89**, 092301 (2002).
[24] STAR Collaboration, C. Adler *et al.*, Phys. Lett. B **595**, 143 (2004).

[25] STAR Collaboration, J. Adams *et al.*, Phys. Rev. Lett. **92**, 052302 (2004).
[26] UA1 Collaboration, C. Albajar *et al.*, Nucl. Phys. **B335**, 261 (1990).
[27] T. Sjöstand *et al.*, Comput. Phys. Commun. **135**, 238 (2001).
[28] I. Vitev (private communication); Phys. Lett. B **562**, 36 (2003).
[29] UA5 Collaboration, G. J. Alner *et al.*, Z. Phys. C: Part. Fields **33**, 1 (1986).
[30] CDF Collaboration, F. Abe *et al.*, Phys. Rev. D **41**, 2330 (1990).
[31] B. H. Sa *et al.*, Phys. Lett. B **537**, 268 (2002).
[32] STAR Collaboration, J. Adams *et al.*, nucl-ex/0311017.
[33] K. Werner, Phys. Rep. **232**, 87 (1993).
[34] B. Andersson *et al.*, Phys. Rep. **97**, 31 (1983).
[35] BRAHMS Collaboration, I. Arsene *et al.*, Phys. Rev. Lett. **91**, 072305 (2003).
[36] PHOBOS Collaboration, B. B. Back *et al.*, Phys. Rev. C **65**, 061901R (2002).
[37] PHENIX Collaboration, K. Adcox *et al.*, Phys. Rev. Lett. **86**, 3500 (2001).
[38] D. Kharzeev, E. Levin, and L. McLerran, Phys. Lett. B **561**, 93 (2003).
[39] STAR Collaboration, J. Adams *et al.*, Phys. Rev. Lett. **91**, 072304 (2003); PHENIX Collaboration, S. S. Adler *et al.*, *ibid.* **91**, 072303 (2003); PHOBOS Collaboration, B. B. Back *et al.*, *ibid.* **91**, 072302 (2003).
[40] PHOBOS Collaboration, B. B. Back *et al.*, Phys. Lett. B **578**, 297 (2004).